Supporting information

Graphene-Based Hybrid Electrical-Electrochemical Point-of-Care Device for Serologic COVID-19 Diagnosis

*Isabela A. Mattioli[1], Karla R. Castro[1], Lucyano J. A. Macedo[1]; Graziela C. Sedenho[1] Mona N Oliveira[2], Iris Todeschini[2], Phelipe M. Vitale[2], Suzete C. Ferreira[4,5], Erika R. Manuli[3,6], Geovana M. Pereira[3], Ester C. Sabino [3,6] and Frank N. Crespilho[1]**

[1]São Carlos Institute of Chemistry, University of São Paulo, São Carlos, SP 13560-970, Brazil
[2] Biolinker Synthetic Biology EIRELI, São Paulo, 05508-000, Brazil
[3] Institute of Tropical Medicine, Faculty of Medicine, University of São Paulo, 05403-000, Brazil
[4] Laboratory of Medical Investigation in Pathogenesis and Targeted Therapy in Onco-Immuno-Hematology (LIM-31), Department of Hematology, Clinical Hospital HCFMUSP, Faculty of Medicine, University of São Paulo, São Paulo, 01246903, Brazil
[5] Division of Research and Transfusion Medicine, São Paulo Hemocentre Pro-Blood Foundation, São Paulo, 05403000, Brazil
[6] LIM-46 HC-FMUSP – Laboratory of Medical Investigation, Clinical Hospital, Faculty of Medicine, University of São Paulo, 01246903, Brazil

Keywords: SARS-CoV-2, COVID-19, serologic detections, graphene, IgG, biosensor

1. EEVD preparation

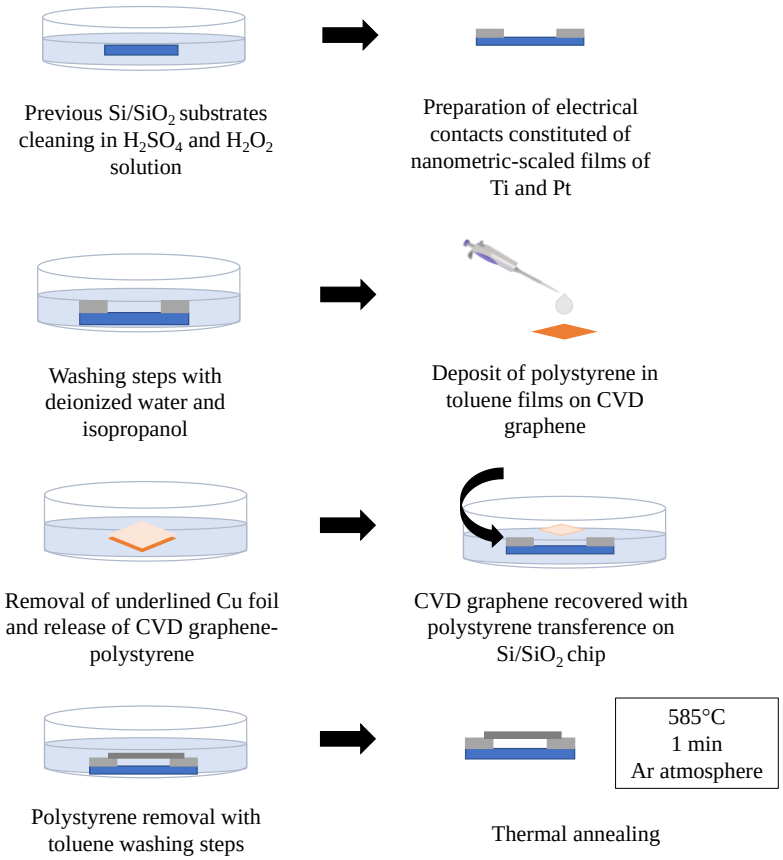

Figure S1 - Pristine graphene EEVD confection. Schematic representation of the steps involved on the monolayer graphene EEVD confection by wet graphene transfer procedure, mediated by polystyrene polymer.

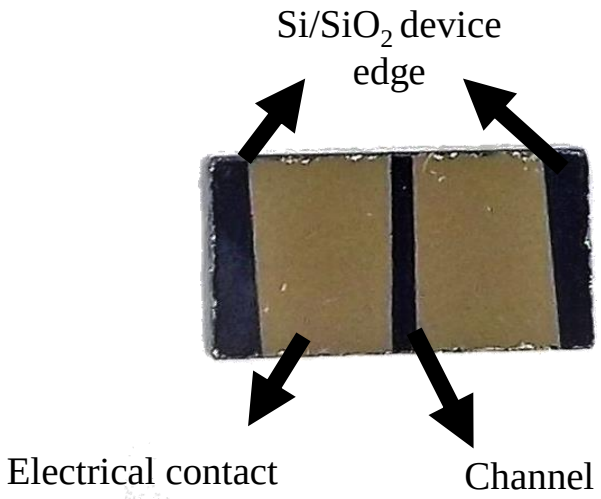

Figure S2 - Pristine graphene EEVD. Photograph of pristine graphene EEVD ready-to-use.

2. Electrochemical etching

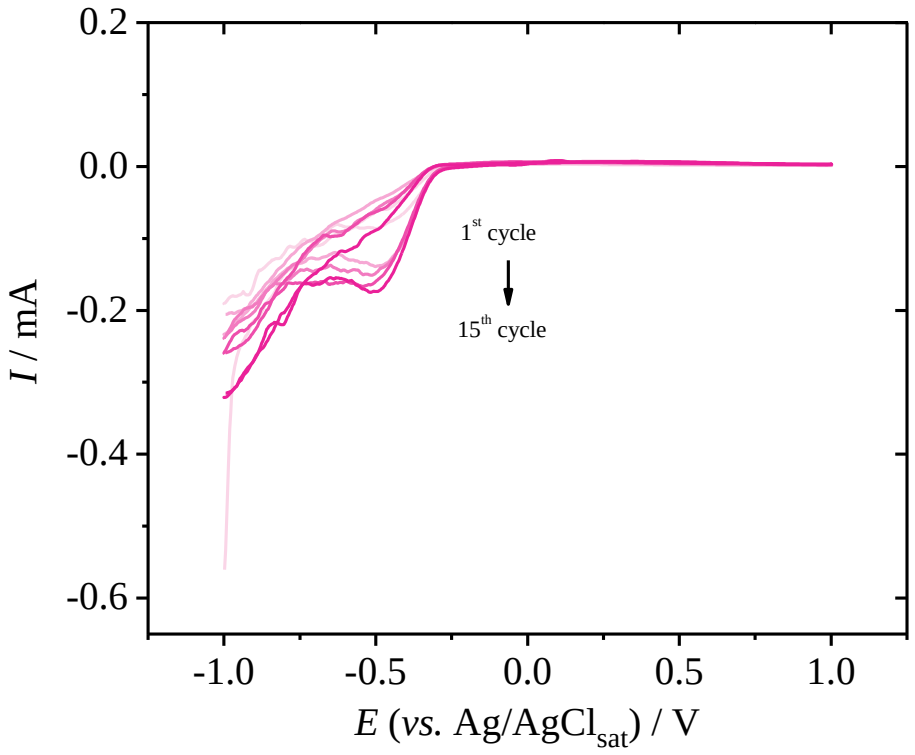

Figure S3 - E-etching of Cu residues. Cyclic voltammograms of Cu residues removal of EEVD graphene surface after wet transfer procedure in 0.1 mol L^{-1} HCl, ν = 100 mV s^{-1}. The color scale varies from clearer pink to darker pink, between 1st, 3rd, 5th, 10th and 15th scans.

3. PNR Electropolymerization

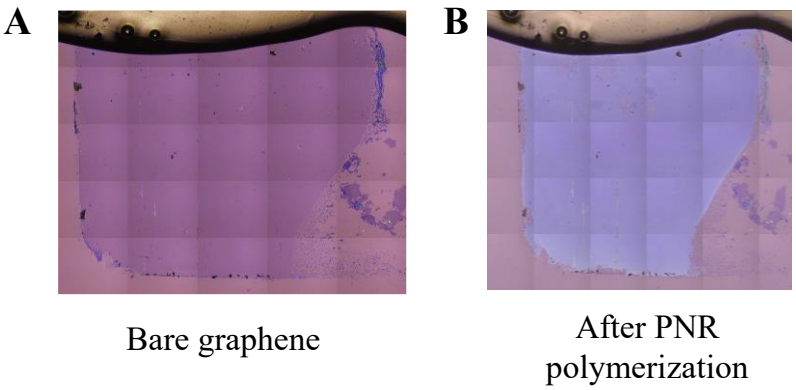

Figure S4 – Optical images of PNR polymerization. Optical image of large area pristine graphene 2D electrode (A) before and (B) after PNR electropolymerization.

The electropolymerization coating of the graphene sheet is also observed by the color contrast in the optical micrographies, where the PNR-coated graphene sheet becomes much less translucid on Si/SiO_2 substrate.

4. Raman Spectroscopy for G-PNR interface

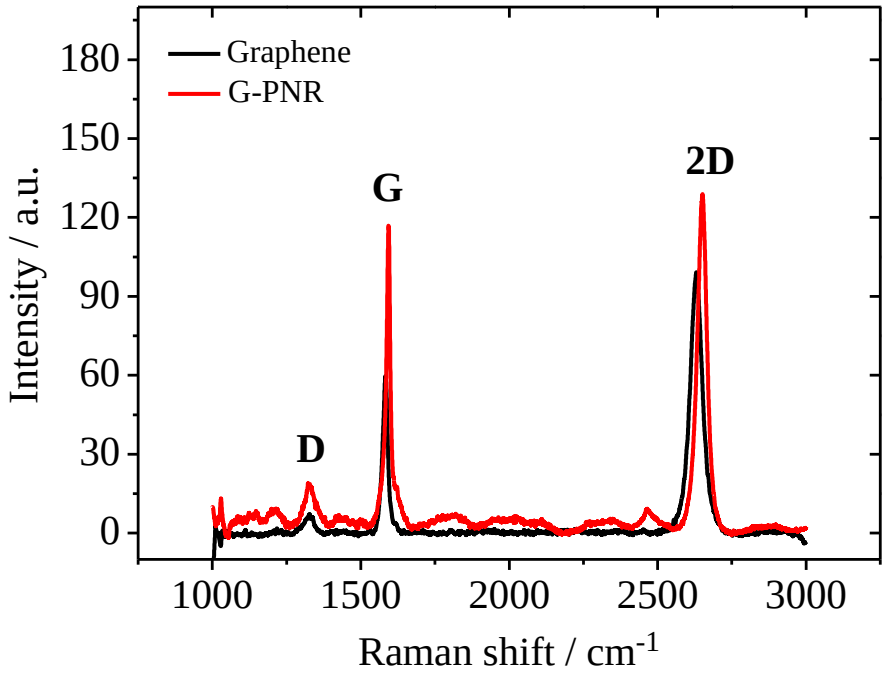

Figure S5 - Raman spectra of graphene and G-PNR electrode surfaces. Comparison between graphene and G-PNR after PNR electropolymerization.

The adsorption of electropolymerized PNR led to the occurrence on *n*-doping onto graphene, according to EEVDs I_{ds} *vs.* V_{ds} results. According to literature, tendencies on *n* or *p*-doping can also be inferred by Raman Spectroscopy, by evaluating G and 2D modes wavenumber shifts.(Wu et al., 2018) However, Raman spectra obtained for both graphene and G-PNR interfaces presented subtle blueshifts of both G and 2D modes, controversially indicating *p*-doping. In fact, evidences of *p*-doping can appear due to sp^3-like defects creation by oxidation of some parts of graphene lattice during electropolymerization by cyclic voltammetry, similarly to what is observed for GO.(Wu et al., 2018) This is corroborated by the increase in D band, generally correlated to point defects on graphene lattice.(Malard et al., 2009) The formation of graphene-polymer composites can also involve stress and strain of graphene lattice and, for this reason, blueshifts are also expected.(Wu et al., 2018)

5. G-PNR Electrochemical Impedance Spectroscopy studies

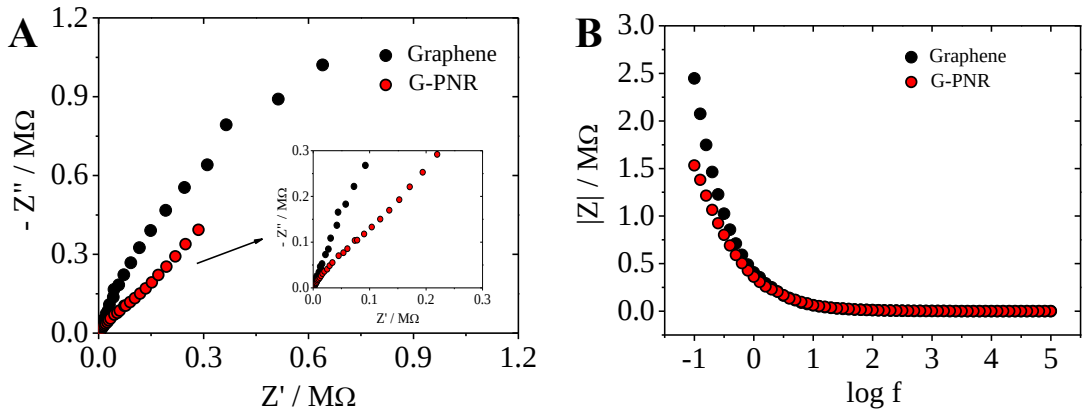

Figure S6 - EIS G-PNR characterization. A) Nyquist plots obtained by EIS for bare graphene (black) and G-PNR (red) EEVD interfaces in a non-electroactive reaction medium (0.01 mol L^{-1} PBS pH 7.4), from 1×10^5 to 0.1 Hz under DC_{pot} = each interface OCP potential, variating with 5 mV of amplitude. B) Impedance modulus curves for graphene (black) and G-PNR (red) interfaces in 0.01 mol L^{-1} PBS pH 7.4, from 1×10^5 to 0.1 Hz, amplitude = 5 mV and DC_{pot} = OCP of each interface

Nyquist plots (Figure S6A) were obtained under OCP potential polarization in a non-electroactive electrolyte, no R_{ct} semicircle was clearly observed, due to the absence of charge transfer processes. For G-PNR, however, a tendency to a semicircle formation can be noticed owing to the faradaic features of electroactive PNR layer. Differences in the plots inclination are generally attributed to capacitive alterations, (Barsoukov and Macdonald, 2013) and in this context, it was possible to infer that PNR modifications decreased the total interfacial capacitance (Figure S6B). This is coherent to the Helmholtz double-layer capacitance model, in which the double-layer capacitance (C_{dl}) is inversely proportional to the double-layer width.(Bard and Faulkner, 2001) This was corroborated by C_{dl} values obtained after best electrochemical circuit fitting (Figure S7): 99.5 ± 5.8 μF cm^{-2} for bare graphene and 84.6 ± 14.1 μF cm^{-2} for G-PNR. Both circuits were simulated based on a typical Randles circuit for electrochemical interfaces. However, ideal double-plate capacitance was replaced by a Constant Phase Element (CPE) in order to take into account interfacial imperfections as roughness, non-homogeneous surface charge distributions, and structural defects.(Barsoukov and Macdonald, 2013) The adsorbed PNR electroactive layer was also considered on equivalent circuit in Figure S7 by adding an extra CPE_{ads} in series to R_{ct}.(Bard and Faulkner, 2001)

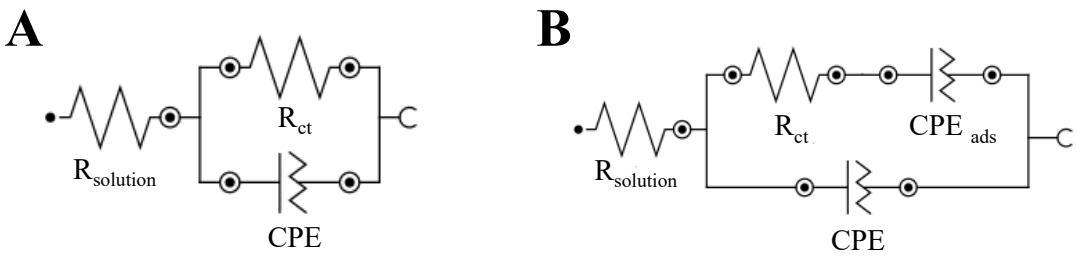

Figure S7 - Equivalent circuits. Equivalent circuits for A) graphene and B) G-PNR interfaces after best electrochemical circuit fitting on NOVA software.

6. UV-Vis for AuNP/RBD bioconjugate

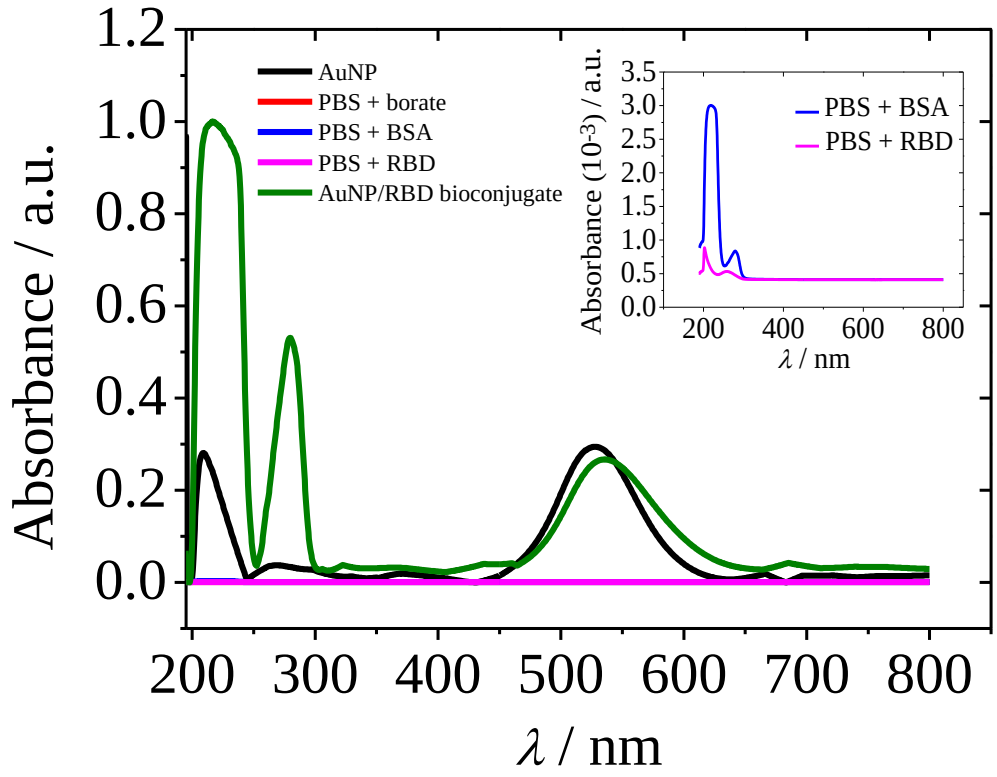

Figure S8 – Bioconjugates UV-Vis spectra. UV-Vis spectra for individual steps of BSA and protein additions for A) AuNP/RBD bioconjugates for the following involved reagents: AuNP (—), PBS + borate buffer (—), PBS + BSA protein (—), PBS + RBD protein (—) and the final AuNP/RBD bioconjugate (—).

All spectra were obtaining considering the spectrum of an aqueous 0.01 mol L^{-1} PBS pH 8 solution as baseline. As expected, AuNP spectrum presented its typical absorption band in 525 nm for AuNP, indicating that insignificant nanoparticles aggregation occurred and the used AuNP may present a diameter value between 15-20 nm.(Cervini et al., 2019) RBD individual spectrum in 0.01 mol L^{-1} PBS pH 8 presented an absorption band in 280 nm, expected due to its proteinaceous nature and the predicted presence of some chromophore residues, as Trp and Tyr.(Nelson and Cox, 2005) This was also valid for individual BSA spectra. Finally, AuNP/RBD spectrum presented a shift in AuNP-525 nm absorption band to higher wavenumbers (537 nm). This redshift is expected for AuNP-based bioconjugates formation and is associated with alterations in the dielectric constant of the electrostatically bonded proteins.(Kozlowski et al., 2018) This is an indicative of interaction establishment between AuNP and RBD and can be used to conclude that the bioconjugate synthesis was successful.

7. TEM characterization for AuNP

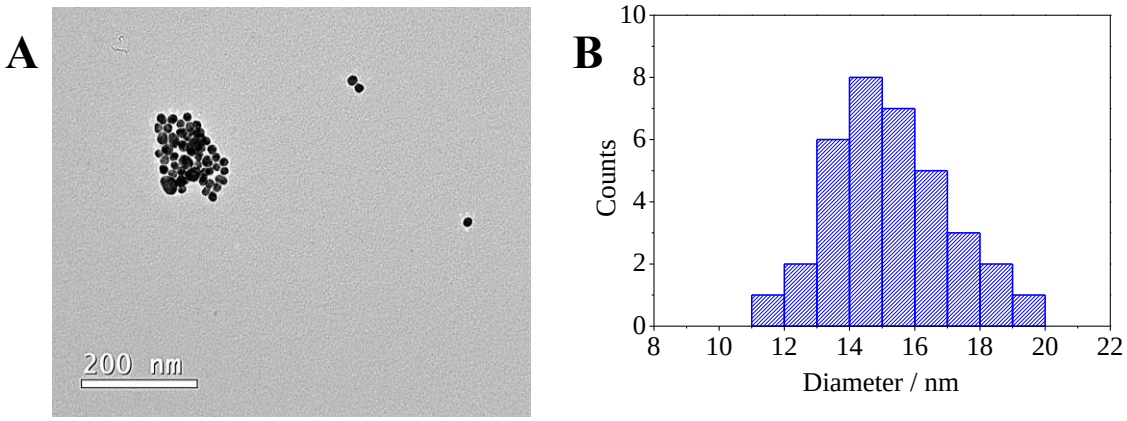

Figure S9 – TEM micrograph for bare AuNP. A) TEM micrograph for bare AuNP colloidal suspension; B) AuNP diameter distribution obtained from TEM micrograph in A), average diameter of (15.3 ± 1.9) nm.

8. Interferents tests

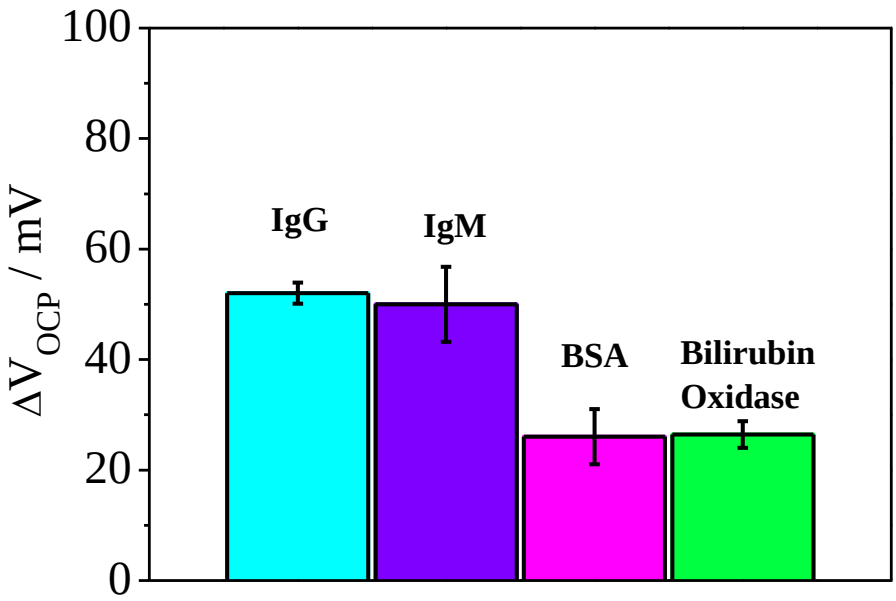

Figure S10 – Possible interferents in IgG detection in human sera samples. Experiments were performed in 0.01 mol L^{-1} PBS pH 7.4 as support electrolyte with 1.0 mg mL^{-1} human IgM, BSA and bilirubin oxidase, respectively.

References

Bard, A.J., Faulkner, L.R., 2001. Electrochemical methods, fundamentals and applications, 2nd ed, John Wiley & Sons, Inc. New York.

Barsoukov, E., Macdonald, J.R., 2013. Impedance Spectroscopy - Theory, Experiment, and Applications. John Wiley & Sons, Inc., Hoboken.

Cervini, P., Mattioli, I.A., Cavalheiro, E.T.G., 2019. RSC Adv. 9, 42306–42315.

Kozlowski, R., Ragupathi, A., Dyer, R.B., 2018. Bioconjug. Chem. 29, 2691–2700.

Malard, L.M., Pimenta, M.A., Dresselhaus, G., Dresselhaus, M.S., 2009. Phys. Rep. 473, 51–87.

Nelson, D.L., Cox, M.M., 2005. Lehninger principles of biochemistry. W. H. Freeman & Company, New York.

Wu, J. Bin, Lin, M.L., Cong, X., Liu, H.N., Tan, P.H., 2018. Chem. Soc. Rev. 47, 1822–1873.